Rheologically Determined Phase Behavior of LCST Blends in the Presence of Spherical Nanoparticles

Amir Gharachorlou and Fatemeh Goharpey*

Department of Polymer Engineering. Amirkabir University of Technology, Tehran, Iran

Received September 18, 2007; Revised Manuscript Received February 21, 2008

ABSTRACT: We have investigated the influence of hard spherical hydrophilic nanoparticles (fumed silica) on the phase behavior of PS/PVME (polystyrene/polyvinyl methyl ether) blend as a compatibilizer. The size of nanoparticles is comparable to the radius of gyration of the polymers and the particles preferentially segregate into one of the polymeric components. Phase separation was assessed using rheological analysis (RMS), differential scanning calorimetry (DSC), and optical microscopy (OM). In order to investigate the kinetics of phase separation in the presence of nanoparticles, time sweep experiments were employed via rheological analysis and OM. A certain composition of PS/PVME was highly concerned to shed light on the dynamic of phase separation, in the presence of nanoparticles, in the unstable region of phase diagram. The phase diagram shifted up nearly 10 °C in the presence of nanoparticles. Blends compatibilized by spherical nanoparticles could provide an interesting and economic alternative to the conventional methods of compatibilization by block copolymers.

Introduction

Phase separation of polymer blends is an open-ended scientific challenge that involves complex combinations of kinetics and thermodynamics. Inducing proper morphologies for multiphase polymer alloys via controlling components compatibility has always seemed to be an important factor in polymer industry. There are four conventional methods for compatibilization of two polymers, namely, (1) cross-link formation between two polymers, (2) forming interpenetrating networks (IPN), (3) changing the chemical structure of the components, and (4) using a third component (mostly copolymers) as compatibilizer.

One area, which has come under intense study, is the role of nanoparticles as potential compatibilizers in blends of immiscible polymers, which can provide an interesting alternative instead of compatibilization by copolymers.

Although there have been several studies on nanocomposite physical and mechanical properties,[1] little data is available on the effect of nanoparticles on the phase diagram and dynamics of polymer blends.

As nanoparticles are added to a polymeric matrix, phase behavior may become more complex. In polymer blends, it has been shown that introducing active filler makes the phase behavior more complex by means of changing the shape of the phase diagram,[2] changing the interaction parameter between two components,[3,4] and increasing or decreasing the phase separation temperature.[2−5]

The effect of nanoparticles on the compatibility of polymer blends and phase separation kinetics has been the subject of several computer simulations by Laradji and McNevin[6] and by Zhu and Ma.[7] Their studies showed that the phase separation slows down in the presence of the nanoparticles. Also, Balazs and co-workers[8−10] have studied the phase separation of a binary polymer blend containing hard particles using both kinetics theory and computer simulations. According to their studies, in case of large preferential affinity to one of polymer components, the particles will concentrate in that component and slow down the growth of the domains in the late stage of spinodal decomposition.

Wang et al.[11] have reported a significant compatibilization by using nanoclay as a compatibilizer for the PP/PS system. Fu et al.[12] used nano-SiO_2 particles with a size of 10–30 nm treated with a hydrophobic coupling agent (nonselective) in the PP/PS system. The nanoparticles caused a kinetics-control compatibilization by reducing the PS phase size at short mixing times through the enhancement in the bending energy of the interface due to diffusion of the particles to the interface. Recently, Ginzburg[5] has provided a simple thermodynamics theory on the influence of the nanoparticles on the phase behavior of the blend of two polymers in which one of the components is preferentially absorbed on the nanoparticles surface. This theory will be discussed in detail later.

When the amount of introduced particles in the blend is small, the majority of the blend stays in the unperturbed state. As the wall-to-wall distance between filler becomes comparable to $2R_g$ (polymer radius of gyration), a network of polydisperse chains forms which bridges neighboring particles. A large number of polydisperse loops and dangling ends are attached to each particle and all the chains are in border layer state.

The effect of introducing fumed silica on the phase behavior of the chlorinated polyethylene and copolymer of ethylene with vinyl acetate with selective adsorption of nanoparticles to one of the components was carried out by Lipatov et al.[3] They showed that at the filler concentrations in which both components transit into border layer state, there is an overall increase in the phase separation temperature.

Krishnamoorti et al.[13,14] employed a two-dimensional concentration and temperature gradient based combinational method in order to clarify the influence of a hydrophobically modified version of the naturally occurring layered silicate montmorillonite on the phase behavior of the PS/PVME. In their studies, the phase behavior remained unaltered by the addition of modified montmorillonite which was attributed to the absence of preferential interaction between layered silicate nanoparticles and the components.

In this study, the blends of PS/PVME were chosen as a polymeric matrix blend. There are many studies on PS/PVME such as the kinetics of phase separation,[15] the separated phase morphology[16,17]segmental mobility,[18]Flory–Huggins interaction parameter dependence on temperature and blend composition,[19]and effect of molecular weight on the phase behavior.[20]

Rheological measurements have been widely used as a sensitive tool to study the phase behavior of polymer blends

* Corresponding Author. E-mail: goharpey@aut.ac.ir, gharachorlou@aut.ac.ir

10.1021/ma7020985 CCC: $40.75
Published on Web 04/12/2008

for several polymeric systems. In the case of compatibilization by copolymers, Chopra et al.[24] have done several studies on the well-characterized SMA/PMMA (styrene−maleic anhydride/poly(methyl methacrylate)) system to rheologically detect the phase diagram for such systems. They have investigated the effect of MA (maleic anhydride) concentration on the rheological and phase behavior of SMA/PMMA blend. They showed that theSMA copolymer containing 14 wt % of MA yielded the highest miscibility in SMA/PMMA blends among all compositions.

Although the literature is rich in flow and shear effect on mixing-demixing phenomena and shear induced morphologies,[25–27] in the present study, because of small strain and very low shear rate exerted on the system, it was assumed that flow does not interfere with thermodynamics and kinetics of the phase separation.[28–36]

DSC technique has been used to assess the liquid–liquid (L−L) demixing temperature of atactic polystyrene/decalin and atactic poly(methyl methacrylate)/1-butanol and cyclohexanol, respectively.[21] Upon cooling, an exothermic heat flow shift was observed and its onset was attributed to liquid–liquid demixing temperature. Kinzer et al.[22] also used DSC techniques to assess solid–liquid demixing (crystallization). DSC techniques have also been employed by Mabrouk et al.[23] to obtain the segregation temperature of the PS/PVME blend.

In polymer blends, changing the composition, temperature and/or pressure can induce phase separation. Nevertheless, disregarding phase separation causes, it occurs either by nucleation and growth mechanism or by spinodal decomposition. When the blend is in its unstable state, a spontaneous process will happen which involves an evolution from homogeneous to disperse phase morphology passing through a percolating cocontinuous structure.

Some research groups have studied the phase separation kinetics and its morphology.[37,38] Time evolutions of the dynamic modulus in metastable and unstable region of the phase diagram have also been extensively investigated in order to correlate the resultant phase-separated morphology with viscoelastic properties of polymer blends.[39] During the phase separation process, the dynamic modulus can show a monotonic decrease or increase depending on the resultant morphologies (cocontinuous or droplet-matrix structure).[30,34,35]

Kapnistos[32] and Polios[30] showed that storage modulus increases with time during the early stage of spinodal decomposition. In the late stages of phase separation, due to the breakup of the interconnectivity, the modulus will gradually decrease.

Time sweep experiments on storage modulus (G') and loss modulus (G'') on PS/PVME were carried out by Kim et al.[26] in order to correlate the morphological changes with rheological behavior of the blend. For both G' and G'', there was a short time increase followed by a decrease in longer time due to the cocontinuous structure.

The main objective of this work is to investigate the effect of spherical hydrophilic nanoparticles (selective-particles) addition on the phase behavior of PS/PVME polymer blend and morphological and kinetics consequences of such nanoparticles addition on the phase behavior of the blend.

Experimental Section

Materials and Sample Preparation. A commercial grade of PS (polystyrene) supplied by Tabriz Petrochemical Co. (GPPS grade 1160) and PVME (polyvinyl methyl ether), Lutonal M40, supplied by BASF Co., were used in this study. Fumed silica nanoparticles (Aerosil 300) with specific surface area of 300 (m^2/g) and average particle size of 7 nm and density of free silanol groups of 2.5 ($SiOH/nm^2$) was used. The basic characteristics of the polymers are listed in Table 1.

Table 1. Characterization of PS and PVME Used in This Study

	M_w (g/mol)	M_n (g/mol)	T_g (°C)	supplier
PS	248000	87000	93.5	Tabriz Petrochemical Co.
PVME	110000	64000	−32	BASF Co.

The PS/PVME/nanoparticle samples, with compositions of 80/20/0, 60/40/0, 40/60/0, 20/80/0, and 80/20/4, 60/40/4, 40/60/4, and 20/80/4, were prepared by continuous mechanical mixing of the components in toluene. The first and second numbers stand for PS and PVME weight fractions respectively, and the last term denotes the volume fraction of the nanoparticle (fumed silica) in the blend. In case of filled samples, the appropriate amount of PS and PVME was codissolved in toluene. Then, enough fumed silica was added to result in a hybrid with a volume fraction of 0.04.

The solvent was evaporated slowly at room temperature for 1 week. Then the samples were put in a vacuum oven for 4 days at 45 °C. The vacuum was applied slowly to prevent any possible bubble formation. Finally, the full vacuum was applied at 70 °C for 24 h in order to remove the residual solvent remaining in the samples. Weighting the samples and making the value match asymptotically to the total weight of the components ensured complete evaporation of the solvent. Considering the chemical sensivity of PVME, utmost cares were taken to prevent its oxidation. This can also be ensured by a simple visual observation of the blend; the sample should look transparent with a slight yellowish hue.[40]

Methods. *Rheological Measurements.* All the rheological measurements were performed by a stress/strain controlled rheometer, UDS 200, made by Paar Physica. The experiments were carried out using disk type parallel plates with 25 mm diameter and 1 mm gap. All the experiments were carried out under a continuous flow of nitrogen gas around the sample pan.

The small amplitude oscillatory shear measurements were performed on the samples as described below:

Isochronal dynamic temperature sweep was carried out by measurement of storage and loss modulus at a fixed frequency (0.04 Hz) which is low enough to lie in the terminal regime[24,32] and a uniform rate of heating (0.5 °C/min) from the homogeneous to the phase separated regime at a certain strain in the linear regime (1%), in order to detect the onset of the phase separation.

In the case of phase separation kinetics, an ∼2 h dynamic time sweep experiment was carried out with a fixed frequency of 0.04 Hz and a given strain of 1% in the phase-separated region for a specific composition of the samples.

All experiments were carried out in the linear regime, as was verified by a preliminary amplitude sweep test.

Optical Microscopy (OM) and Scanning Electron Microscopy (SEM). Optical microscopy samples were also prepared as mentioned earlier. However, the sample thickness for OM was approximately 10 μm. Thicker samples could not be used, since they become so turbid due to a large difference in the refractive index between PS and PVME.

The optical microscopy (Leica DMRX) was used to determine turbidity temperature in temperature sweep mode and the morphological changes at constant temperature. A CCD camera mounted directly on the microscope allowed the recording of blends structure evolutions in real time. The sample was placed in a hot stage (Linkam LTS350) which was controlled by the hot stage controller (Linkam CI 94). The cloud points of PS/PVME and PS/PVME/Nano samples were determined by the optical microscopy observation coupled with hot stage. The heating rate was set to 0.5 °C/min for all samples in the cloud point's temperature measurements. Fresh nitrogen gas was circulated in the heating chamber of OM to avoid any possible thermal degradation. Then the morphological changes in unstable region of the phase diagram at constant temperature were observed.

SEM (Phillips XL30) images were used to study the morphological changes in PS/PVME blends with and without silica nanopar-

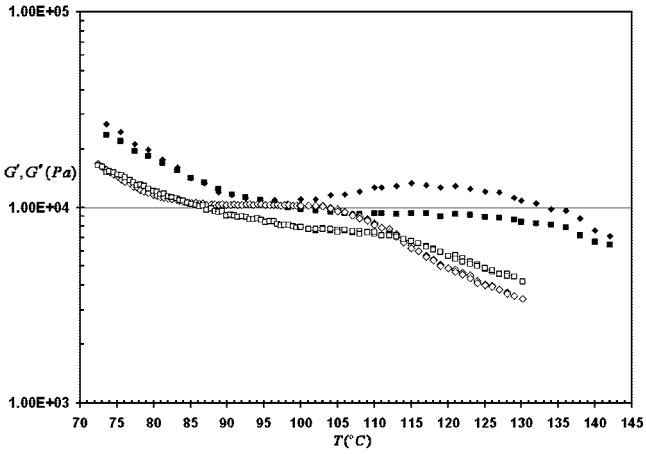

Figure 1. Isochronal (f = 0.04 Hz) dynamic temperature sweep performed at 1% strain with a heating rate of 0.5 °C/min. Key: 40/60/0 (G'), ◇; 40/60/0(G''), □; 40/60/4(G'), ♦; 40/60/4(G''), ■.

ticles. The samples were cryogenically fractured across the thickness in liquid Nitrogen and the fracture surfaces were etched by the methanol for 1 min, which preferentially etched out the PVME phase. Then the samples were sputter-coated with a thin layer of gold.

Element mapping on Si was conducted with the same scanning electron microscope equipped with an energy dispersive X-ray spectroscopy (EDX) (Oxford 7538). As the scan was performed, if the EDX detector observed counts for the desired element, a bright dot would be displayed on the monitor. It is worth to mention that the dot map is only qualitive, conveying the spatial location of selected constituents but not the amount present.

Transmission Electron Microscopy (TEM). Transmission electron microscopy (TEM) images of the samples were obtained with a Philips EM 208 transmission electron microscope operating at 100 keV. The samples were prepared for cross sectional TEM by cryomicrotoming (using a diamond knife) epoxy-supported thick films into ~60 nm slices at −100 °C to prevent any possible morphological changes during cutting.

The polymer latent ability to degrade selectively in the electron beam causes the contrast between the phases in the PS/PVME system. The PVME is more electronegative (due to its ether bond) and absorbed electrons more easily. Thus the PVME-rich phase forms light regions while the dark regions are PS-rich phase. This image would not change significantly for ~20 min.

Differential Scanning Calorimetry (DSC). The DSC technique was employed (Dupont 2000) to obtain the binodal temperature in PS/PVME and PS/PVME/nanoparticles samples. All the experiments were done under a continuous flow of nitrogen gas around the sample pan to prevent thermal degradation. Prior to measurements, the baseline was established using two empty pans.

The samples were placed in an aluminum pan and heated up to 180 °C at a heating rate of 2 °C/min. there was a sudden heat capacity shift due to the heat exchange during the phase separation process, which were attributed to the demixing temperature of PS/PVME and PS/PVME/Nano samples. The phase separation temperature was determined from the first heating run for all samples. Samples were prepared with the same thermal history; therefore, the temperature obtained from first-run heating was not affected by the difference in thermal history of the samples.

Results and Discussions

Rheology. Rheological measurement is a reliable method for phase behavior analysis. However, to our best knowledge, this is the first time that such a method is being employed in order to detect the effect of nanoparticle addition on the phase behavior of a binary polymer blends.

A typical curve of elastic modulus (G') and loss modulus (G'') versus temperature is shown in Figure 1 for the 40/60/0 and 40/60/4 (PS/PVME/Nano) blend samples.

In both cases, at low temperatures the elastic modulus (G') decreases with temperature rise. This was attributed to the greater mobility of the polymer chains as the system moves away from its glass-transition temperature. In the vicinity of phase separation temperature, there is always a competition between mobility and thermodynamics. As the temperature reaches the phase segregation temperature, the thermodynamic forces become dominant and increase the magnitude of G' (upturn in G' curve) by formation of dynamic domains, rich in the hard PS component of the blend.

At low particle loading (4 vol % nanoparticles) the qualitative features of viscoelastic behavior remains unaffected by addition of nanoparticles and there is only an overall increase in the magnitude of storage modulus (G').

In case of filled samples, the PVME-rich phase consists of PVME chains absorbed on nanoparticles surface. The absorbed polymer segments show a reduced mobility near the particle surface. This absorbed layer provides regions with lower mobility to which different segments are able to reach within the longest relaxation time of the polymer. This slowing down of the overall dynamics of the polymer segments leads to an overall increase in the magnitude of G' in the 40/60/4 blend as compared to the neat blend of PS/PVME, at low frequencies (~0.04 Hz).[41]

By further increase in temperature, the reappearance of phenomena controlled by mobility forces were observed and G' decreased once again. The inflection point of G' versus temperature curve is referred to as rheological phase separation temperature (T_{Rheo}). This assignment is empirical and is not based on a specific physical background.

G'', also exhibits similar behavior but with much less sensitivity and a phase lag. This phenomenon is more obvious in the presence of nanoparticles i.e. in 40/60/4 blend. The higher sensitivity of G' is attributed to the elastic origin of the stress induced to the system by concentration fluctuations. In mechanical analogy (Maxwell model), the elastic component responds faster and more significantly to a given deformation, as compared to the viscous component.

In the present study, the qualitative features of the storage modulus remained unaffected at low particle loading (Figure 1). These results are in good accordance with Ganesan's et al.[41] computer simulations of polymeric composites containing nanospherical particles.

In the 40/60/4 blend, the inflection point shifts to a higher temperature. This represents the effect of nanoparticle content on the interaction parameter and confirms that blends containing 4% volume of nanoparticles are more miscible. The same behavior was observed in all other compositions.

Figure 2 depicts the G' versus T behavior of PS/PVME/Nano blends in various compositions. Like the neat PS/PVME blend, the behaviors of the blends differ significantly in different compositions. This figure also shows that the temperature range in which the upturn occurs, and its magnitude are strongly affected by the blend composition. In fact, changing the composition, changes the distance of the effective blends T_gs from the individual components T_g, and this will change the dynamic asymmetry of the blend, which is the main cause of the observed viscoelastic behavior.[42]

For the quantitative studies of phase separation, we turned to the theoretical approach of Ajii and Choplin[43] which is the extension of the earlier theories of Fredrickson and Larson[44] for block copolymer melts near the order–disorder transition, to the case of homopolymer blends.

The mean field theory has been used to derive the critical contribution to the shear stress for near critical polymer mixtures. The dynamic storage and loss modulus were obtained after integration over the whole wave-factor space and also using eq 1

$$G^* = \sigma^*/\gamma^* \tag{1}$$

$$G'(\omega) = \frac{k_B T \omega^2}{15\pi^2}\int_0^{k_c} \frac{k^6 S_0^{\,2}(k)}{\omega^2 + 4\bar{\omega}^2(k)}\left[\frac{\partial S_0^{\,-1}(k)}{\partial k^2}\right]^2 \mathrm{d}k \tag{2}$$

$$G''(\omega) = \frac{2k_B T \omega}{15\pi^2}\int_0^{k_c} \frac{k^6 S_0^{\,2}(k)\bar{\omega}(k)}{\omega^2 + 4\bar{\omega}^2(k)}\left[\frac{\partial S_0^{\,-1}(k)}{\partial k^2}\right]^2 \mathrm{d}k \tag{3}$$

where $\bar{\omega}(k) = k^2 S_0^{\,-1}(k)\lambda(k)$, $S_0(k)$ is the static structure factor, $\lambda(k)$ is the Onsager coefficient, and k is the wave factor. The above equation could be applied using the De Gennes mean field structure in the case of binary polymer blends:[45]

$$\frac{1}{S_0(k)} = \frac{1}{\phi N_1 g_1(k)} + \frac{1}{(1-\phi)N_2 g_2(k)} - 2\chi \tag{4}$$

where N_i is the number of statistical segments, $g_i(k)$ is the Debye function and χ is the interaction parameter. The expression for the Onsager coefficient proposed by Binder[45] is

$$\frac{1}{\lambda(k)} = \frac{1}{\phi b_1^{\,2} W_1 g_1(k)} + \frac{1}{(1-\phi) b_2^{\,2} W_2 g_2(k)} \tag{5}$$

with b_i being the statistical segment length for species i and W_i being the rate of its reorientation:

$$W_i = 3\pi k_B T/\xi_i \tag{6}$$

with ξ being the monomeric friction coefficient. For the terminal one-phase region near the critical point, we have:

$$G''(\omega) = \frac{k_B T \omega}{240\pi}\left[\frac{1}{3}\left\{\frac{R_{g1}^{\,2}}{\phi N_1} + \frac{R_{g2}^{\,2}}{(1-\phi)N_2}\right\}\right]^{-1/2}\left[\frac{1}{\phi b_1^{\,2} W_1} + \frac{1}{(1-\phi) b_2^{\,2} W_2}\right][2(\chi_s - \chi)]^{-1/2} \tag{7}$$

$$G'(\omega) = \frac{k_B T \omega}{1920\pi}\left[\frac{1}{3}\left\{\frac{R_{g1}^{\,2}}{\phi N_1} + \frac{R_{g2}^{\,2}}{(1-\phi)N_2}\right\}\right]^{-1/2}\left[\frac{1}{\phi b_1^{\,2} W_1} + \frac{1}{(1-\phi) b_2^{\,2} W_2}\right]^2[2(\chi_s - \chi)]^{-5/2} \tag{8}$$

In the above equations, χ_s stands for the interaction parameter at the spinodal, i.e., when $S_0^{\,-1}(0) = 0$, and R_{gi} is the radius of gyration for species i defined as $R_{gi}^{\,2} = N_i a_i^{\,2}/6$. Using the above equation, the ratio can be calculated by substituting the values of the defined parameters.

$$\frac{G'(\omega)}{[G''(\omega)]^2} = \frac{30\pi}{k_B T}\left\{\frac{b_1^{\,2}}{36\phi} + \frac{b_2^{\,2}}{36(1-\phi)}\right\}^{3/2}(\chi_s - \chi)^{-3/2} \tag{9}$$

The noticeable point of eq 9 is that both the monomeric friction coefficient and the frequency dependence are eliminated. Assuming that the interaction parameter is given by $\chi = A + B/T$, there would be a linear dependence of $((G'')^2/G'T))^{2/3}$ vs $1/T$, for which the interception with the $1/T$ axis is denoted as the reciprocal to the spinodal temperature, T_s.

Figure 3 shows the typical representation of data for the 40/60/0 and 40/60/4 PS/PVME/Nano blends where the linear range is observed in the phase transitional region, and the corresponding lines give an estimate of spinodal temperature. The selection of linear region seems to be crucial for determination of T_s. In the present study, the error of measurement is about ±3 °C.

Demixing Temperature Determined by DSC Technique. Figure 4 shows the differential scanning calorimetric (DSC) thermogram of the 40/60/0 and 40/60/4 blends. As can be seen, there is a dramatic shift in DSC thermogram, far from the component's T_gs, which was taken as the signature of phase segregation in the presence of the nanoparticles. As long as the blend remained in the miscible region PS/PVME/Nano blends absorb energy and there is no sudden heat capacity change in the diagram. When the blend reaches the segregation temperature, there is an energy exchange due to the phase segregation

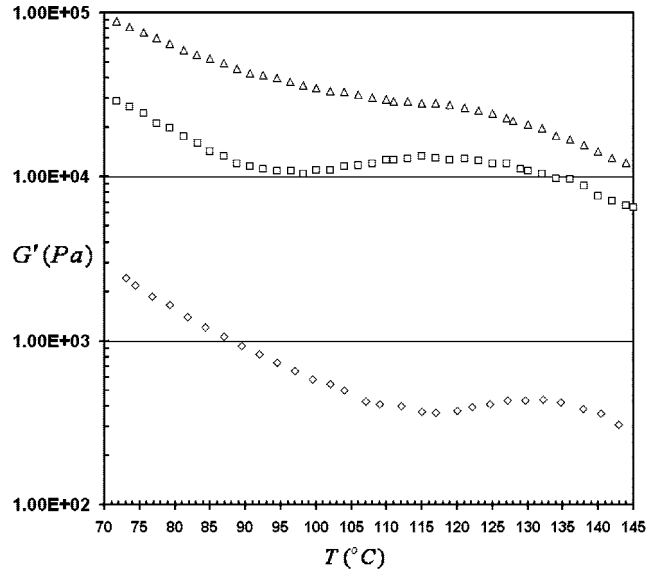

Figure 2. Temperature dependence of storage modulus of 4 vol % filled samples at various PS/PVME blend compositions: 20/80 (◇); 40/60 (□); 60/40 (Δ). Measured at $f = 0.04$ Hz and with 1% strain and a heating rate of 0.5 °C/min.

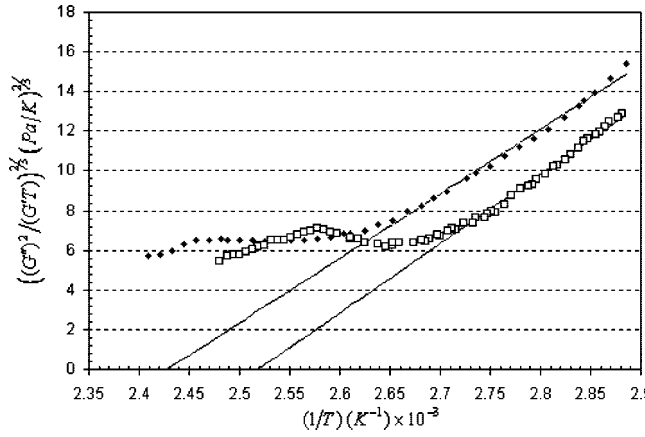

Figure 3. Quantitative evaluation of the viscoelastic behavior of 40/60/0: (□) and 40/60/4: (♦); blends near the phase separation and determination of the spinodal temperature.

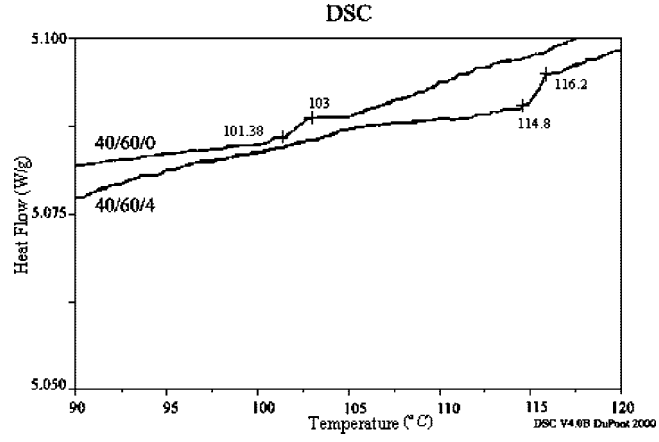

Figure 4. Typical DSC curves with a heating rate of 2 °C/min indicating the phase separation temperature of the blends. The blend composition is mentioned near the corresponding curve.

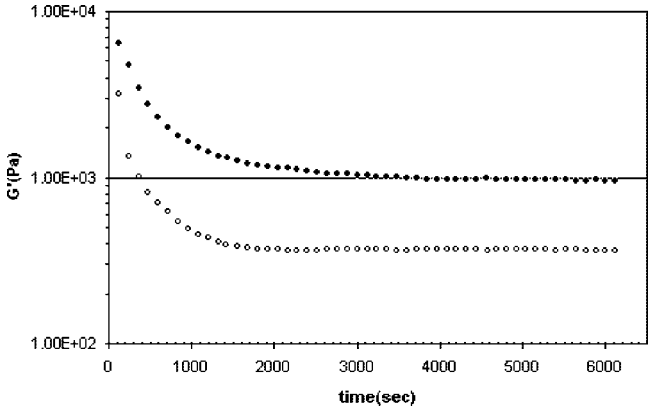

Figure 5. Time evolution of the storage modulus at frequency = 0.04 Hz and with 1% strain for 40/60/4 (•), T = 142 °C; 40/60/0 (○), T = 126 °C.

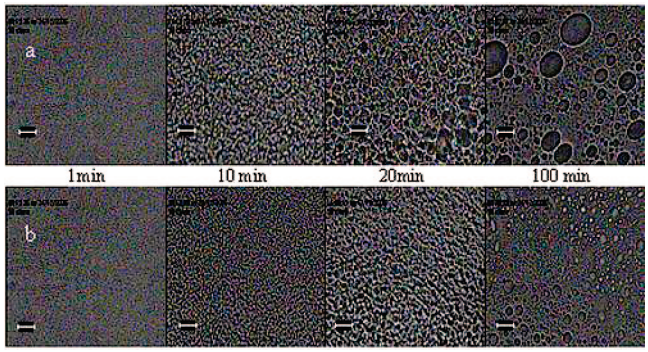

Figure 6. OM images of 40/60/0, T = 126 °C (a), and 40/60/4, T = 142 °C (b), blends (the white scale bar corresponds to 50 μm).

process.[20] Here instead of employing conventional T_gs analysis (a single glass-transition temperature or two distinct T_gs corresponding to those of respective components), the shift in the vicinity of phase separation has been attributed to the phase separation temperature. To our best knowledge, this is the first time that this technique was used to assess the segregation temperature of a nanocomposite polymeric blend.

In both cases there is a good agreement between DSC results and those obtained from other techniques, Figure 8.

Kinetics. *Time Sweep.* In order to investigate the phase separation kinetics, time sweep experiments were carried out with fixed frequency of 0.04 Hz and strain of 1%, for a quench depth ($\Delta T = T - T_{binodal}$) of 32 °C on the 40/60/0 and 40/60/4 (PS/PVME/Nano) blends at 126 and 142 °C, respectively. The above temperatures were chosen because they have the same quench depth into two-phase region. As a result, the thermodynamics forces, which are responsible for phase separation, are almost the same.

The 40/60/0 and 40/60/4 blends at 126 and 142 °C both locate in the unstable region of the phase diagram. In this situation, a sudden growth of concentration fluctuation creates a highly interconnected structure.

Clearly, in both cases the storage modulus at above-mentioned temperatures decreases with time but the decreasing magnitude and the rate of this reduction is strongly affected by the presence of the nanoparticles (Figure 5). We can compare the rheological response with OM images of these samples, which will be presented in next section (Figure 6). It takes less than 1200 s for the storage modulus of the 40/60/0 blend to reach its saturated stage while the time needed for such transition for 40/60/4 blend would be more than 2500 s. At this stage, there would be no obvious decrease in the magnitude of storage

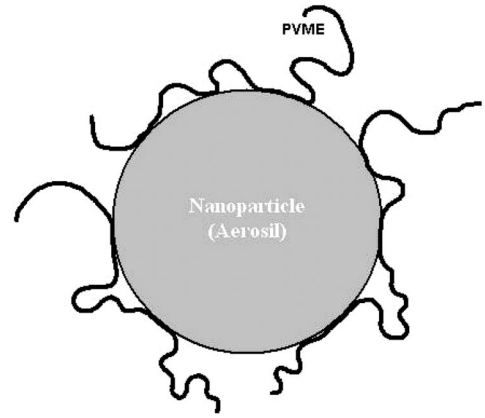

Figure 7. Schematic representation of nanoparticles covered with PVME chains.

modulus. In the late stage, when the concentration fluctuation becomes almost saturated and the composition of both phases remains approximately constant, the interfacial phenomena become dominant. However the storage modulus continuously decreases because of the phase domain coarsening or coalescence and/or breaking up of the highly interconnected bicontinuous structures.

This could be also more appreciated by a nonphysical network model.[31] For a network structure, the elastic behavior is an increasing function of number of cross-linkings per unit volume. By analogy, the interconnected structure of SD could be assumed as a nonphysical network. As time passes, the number of interconnections decrease and consequently, the contribution of the cocontinuous part of the structure to G' is decreased. This explains why loss of the interconnectivity could lead to a decrease in the storage modulus.[28] It should also be noted that PVME is more polar than PS as indicated by comparing the dispersive and polar components of PVME[46](δ_d = 15.5 MPa$^{1/2}$ and δ_p = 7.1 MPa$^{1/2}$) with that of PS[47] (δ_d = 18.1 MPa$^{1/2}$ and δ_p = 1.1 MPa$^{1/2}$). Therefore hydrophilic fumed silica is expected to be preferentially absorbed into PVME.

In the blends containing 4% of Aerosil, the existence of low mobility regions absorbed on particles slows down the phase separation process. It seems that nanoparticles act like retarders in the SD process and the interconnected network remains in its initial state for a longer period of time. Aerosil particles, which do not behave as surfactants, prefer to be in the bulk of the PVME-rich phase (selective absorption). Actually they would represent a network of obstacles for the coarsing of the interfaces and slow down the phase separation process.[8–10] Similar results were also observed with OM analysis, which will be discussed in the next section.

Optical Microscopy (Turbidity Temperature Measurements). In the case of polymers, considering their high molecular weights, the chains dynamics is so slow that the interpenetrating structure in the early and intermediate stages could remain for even several hours which make structure changes detectable by classical techniques such as optical microscopy (OM).

We have employed the OM technique coupled with a hot stage, to have deep insight into the morphology development during the phase separation at constant temperature. In order to have good correlation with storage modulus time sweep experiments, the temperature was kept at the constant value of 126 °C for neat blends and 142 °C for the blend containing 4 vol % Aerosil.

Figure 6 shows the morphological development by time in the unstable region of the phase diagram for 40/60/0 and 40/60/4 blends. As depicted in this figure, in the 40/60/4 sample, the transition from interpenetrated structure to matrix-disperse

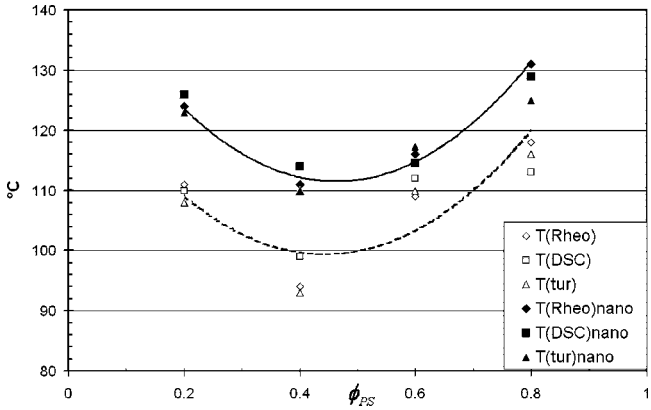

Figure 8. Phase diagram for the PS/PVME/Nano and PS/PVME blends obtained from various techniques: rheological measurements, DSC and turbidity measurements. The figure shows the good agreement between different methods. (Lines are only guides for the eyes.)

is slower than the 40/60/0 sample. After 100 min, as the phase separation is in its final stage, a drastic reduction of PS phase size and a homogeneous size distribution were observed by introducing nanoparticles (Aerosil). This behavior was previously observed in PS/PVME blend in the presence of nonselective layered silicate nanoparticles.[13] This slow down in the phase separation process becomes more pronounced because of the selective interaction of one of the polymer components with the nanoparticles surface. Interestingly enough these observations are in good agreement with the storage modulus vs time results.

The optical microscopy technique was also used to determine turbidity temperature in the temperature sweep mode. In order to have good comparison with rheological analysis, heating rate was adjusted to 0.5 °C/min. In each case, the first sign of phase separation morphology development was attributed to the binodal temperature of the blend.

The results obtained by this technique are more reliable comparing to common turbidity measurement techniques based on the naked eye observation.

Phase Diagram. Figure 8 shows the phase diagram of PS/PVME with and without silica nanoparticles. As seen, there is a good agreement between the phase separation temperatures determined by different techniques. The LCST phase diagram shifts toward a higher temperature in the presence of silica nanoparticles.

Recently Ginzburg[5] proposed a simple model considering a binary mixture of two homopolymers A and B and spherical nanoparticles with prefential absorption into polymer A (covered with an A-polymer layer) and tried to find out a simple comprehensive theory for polymer blends/nanoparticles mixture (Figure 7).

He employed the equation below for free energy (per unit volume) in order to calculate the influence of the nanoparticles on the location of the phase diagram.

$$F = F_{\text{pol}} + F_{\text{part}} + F_{\text{int}} \tag{10}$$

$$F_{\text{pol}} = \frac{(1-\psi)\phi}{N}\ln\left[\frac{(1-\psi)\phi}{N}\right] + \frac{(1-\psi)(1-\phi)}{N}\ln\left[\frac{(1-\psi)(1-\phi)}{N}\right] + \chi(1-\psi)^2\phi(1-\phi) \tag{11}$$

$$F_{\text{part}} = \frac{\psi}{\upsilon_p}\left[\ln\psi + p\left(\frac{R_p}{r_o}\right)\frac{4\psi - 3\psi^2}{(1-\psi)^2}\right] \tag{12}$$

$$F_{\text{int}} = \frac{\psi}{\upsilon_p}(1-\psi)p\left(\frac{R_p}{r_0}\right)\frac{3R_p^2}{2Nr_0^2} + \chi\psi\left[\frac{r_0}{R_p}\right](1-\psi)(1-\phi) \tag{13}$$

The first term in eq 10 is simply the Flory–Huggins free energy, which has been modified to take the volume occupied by nanoparticles into account. The second term in eq 10 describes the entropic contribution of particles themselves in two different terms: ideal and nonideal "entropic free energy" of hard spheres. The third term in eq 10 shows the entropic and enthalpic interactions between the particles and polymer.

Here R_p, υ_p, Ψ, N, Φ, χ, and r_0 are spherical particles radius, nanoparticle volume, nanoparticle volume fraction, degree of polymerization, blend composition, Flory–Huggins interaction parameter and monomer radius respectively. $P(R_p/r_0)$ is an "interpolating factor" that eliminates the hard-sphere correction. In our work $R_p/r_0 \gg 1$; thus, this value is high enough to consider the hard-sphere correction that is $P \rightarrow 1$.

The first term in eq 13 has an entropic contribution. There is a significant increase in the % trans in the region close to nanoparticles.[48] It is assumed that each polymer chain acquires stretching free energy every time it encounters a particle. This energy is called "entropic surface tension" and is given by:

$$h \sim 3R_P/2Nr_0^2 \tag{14}$$

The second term in 13 describes the enthalpic contribution that is proportional to the number of contacts between the particle surface and B-monomer that becomes smaller as the particle radius increases.

Introduction of nanoparticles made a large number of reasonably flexible PVME chains absorb onto their surface. The preferred localization of these PVME covered nanoparticles is dictated by the thermodynamic forces.

Block copolymers have been highly considered as templates to control the location of nanoparticles within the polymer matrix.[49] There is a simple and common procedure to control the location of nanoparticles within the A or B domains of the block copolymer by variation of a single parameter, the surface coverage and chemistry of nanoparticles. In general, if the nanoparticles are compatibilized to just one of the components (selective particles), their immiscibility with one of the domain and their miscibility with the other one, provides a strong driving force for the particles to preferentially segregate at the center of their preferred phase while particles compatible with both components (nonselective or neutral) work similar to surfactants and diffuse to the interface between the two domains.

The nanoparticles distribution and location were studied using an X-ray mapping technique and TEM images. The X-ray mapping technique was recently employed by Liu and coworkers to study the silica nanoparticle distribution in a chitosan−silica complex membrane.[50] Whenever the constituent is present at low concentration, the recording condition should be adjusted carefully so that the dot "blooms" and becomes more readily visible.

Figure 9 shows the EDX mapping spectra of the 40/60/4 (PS/PVME/Nano) sample at 130 °C for 100 min. Under this condition, the sample undergoes spinodal decomposition and shows a cocontinuous structure as it could be seen in Figure 11b. In addition to the unfavorable enthalpy of interactions between PS and PVME covered silica nanoparticles, an entropic barrier must be overcome by PS to reach the PVME stretched chains coated silica nanoparticles. Therefore, particles covered with PVME chains are expected to be strongly driven into the bulk of PVME-rich domains away from interface to lower their enthalpy by segregating into the corresponding portions of the blend.

In addition to selective localization of silica nanoparticles into PVME domains (when the PVME was extracted out from the samples by methanol, there was nearly no trace of Si in EDX mapping image) the homogeneous distribution of silica nanoparticles in the PVME rich phase was observed. In support to above arguments come our TEM results (Figure 10). The dark regions correspond to the PS-rich phase while the bright regions

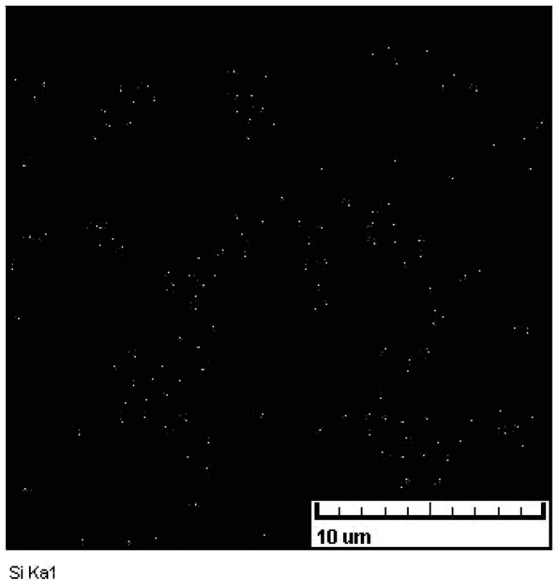

Figure 9. X-ray Si-mapping image of 40/60/4 (as explained in the text). The bright spots are corresponding to Si elements.

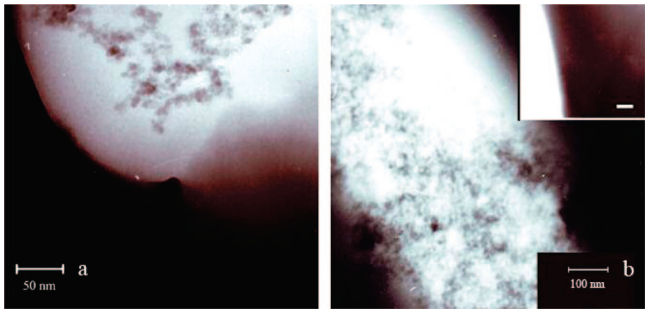

Figure 10. TEM micrograph of 40/60/4 (PS/PVME/Nano) sample annealed at 130 °C for 100 min. Parts a and b correspond to different sample areas and magnification. The scale bar is 50 nm in the small window.

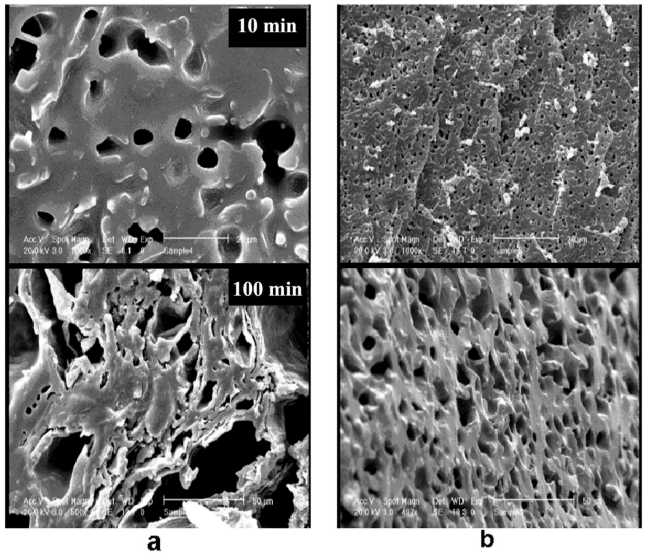

Figure 11. SEM images for 40/60/0 PS/PVME/Nano (a) and 40/60/4 PS/PVME/Nano (b), at 130 °C.

correspond to PVME-rich phase.[51] Note that silica nanoparticles are observed as black dots, within the bright PVME-rich phase. From Figure 10, it is clear that the particles are distributed roughly around the central region of PVME-rich phase.

Turning back to the theory, the high entropy of such small particles (eq 12) and the replacement of some PVME homopolymer with PVME covered nanoparticles reduces the enthalpic portion of free energy by decreasing the number of unfavorable PS/PVME interaction.

On the other hand, $N_{PVMV}^{1/2} \gg R_p$, so the role of "entropic surface tension" (entropic penalty) for particles in the polymer is not quite as considerable. Thus, the nanoparticles should act as a compatibilizer for the polymer blend and should shift the phase separation temperature toward higher temperatures.[5]

In particular, Ginzburg found that

$$\frac{(\chi N)_{sp}(\psi)}{(\chi N)_{sp}(0)} \leq \frac{1}{1-\psi} \approx 1+\psi \tag{15}$$

In the above equation, if we assume that $\chi = B/T$, then one can obtain the effective decrease in the spinodal temperature of a binary blend in the presence of nanoparticles:

$$\left[\frac{\Delta T}{T}\right]_{sp} = -\left[\frac{\Delta(\chi N)}{\chi N}\right]_{sp} \approx -\psi \tag{16}$$

Equation 16 shows that for a binary blend with a critical temperature of 396 K, addition of 4 vol % of nanoparticles can reduce the critical temperature up to 16 deg. In our work, addition of 4 vol % fumed silica caused the spinodal temperature to shift from 396 to 413 K in the 40/60/4 samples. Therefore, the model successfully predicts the effects of nanoparticles as a compatibilizer in this system.

Figure 11 shows SEM images of thick samples (1 mm) of the 40/60/0 and 40/60/4 (PS/PVME/Nano) at two different phase separation times at 135 °C. The dark regions in the SEM images represent PVME-rich phase, which was extracted out by methanol. As expected, it can be seen that the nanoparticles significantly change the interdomain spacing in cocontinuous structures. Nanoparticles shift the phase separation temperature to higher temperatures as a thermodynamic compatibilizer. Therefore in the samples containing nanoparticles the quench depth would be different and clearly the phase separation morphology would also differ. These images could be another supporting evidence to clarify the effect of nanoparticles as compatibilizers, which was discussed in detail before.

Conclusions

In this study, we have shown that even a low percentage of spherical hydrophilic nanoparticles can significantly affect the phase behavior and the phase-separated morphology of the PS/PVME blends.

As expected from the Ginzburg thermodynamic model, it is found that when PVME chains cover the nanoparticles, the addition of nanoparticles shifts the phase separation temperature into higher temperatures. This is due to the reduction of unfavorable PS/PVME interaction by absorption of some of the PVME chains on nanoparticles surface. Also the addition of small particles with such high entropy would assist the free energy reduction and the stability of the homogeneous phase. When the Aerosil particles are added into the PS/PVME blends, they slow down the phase separation dynamics by absorbing the chains on their surface and retarding the domains growth. Better understanding of these complicate systems remains a challenge for further studies.

Acknowledgment. The authors thank Mrs. T. Samaee Yekta for the optical microscopy images and Mr. Rezaee from Tarbiat Modares University who helped us a lot with the SEM images. We would like to thank Sadegh Behdad, Shahed Khayatzadeh, Ehsan R. Mafi, and Amir Fathi for critical reading of the manuscript.

It is also our pleasure to thank anonymous reviewers for their stimulating suggestions and remarks.

References and Notes

(1) (a) Manias, E.; Touny, A.; Wu, L.; Strawhecker, K.; Lu, B.; Chung, T. C. *Chem. Mater.* **2001**, *13*, 3516–3523. (b) Gangopadhyay, R.; De, A. *Chem. Mater.* **2000**, *12*, 608–622. (c) Moniruzzaman, M.; Winey, K. I. *Macromolecules* **2006**, *39*, 5194–5205.
(2) Nesterov, A. E.; Lipatov, Y. S.; Horichko, V. V.; Gritsenko, O. T. *Polymer* **1992**, *33*, 619–622.
(3) Nesterov, A. E.; Lipatov, Y. S. *Polym. Commun.* **1999**, *40*, 1347–1349.
(4) Lipatov, Y. S.; Nesterov, A. E.; Ignatova, T. D.; Nesterov, D. A. *Polymer* **2002**, *43*, 875–880.
(5) Ginzburg, V. V. *Macromolecules* **2005**, *38*, 2362–2367.
(6) Laradji, M.; MacNevin, G. J. *Chem. Phys.* **2003**, *119*, 2275–2284.
(7) Zhu, Y. J.; Ma, Y. Q. *Phys. Rev. E* **2003**, *67*, 041503.
(8) Ginzburg, V. V.; Qiu, F.; Paniconi, M.; Peng, G.; Jasnow, D.; Balazs, *A. C. Phys. Rev. Lett.* **1999**, *82*, 4026–4029.
(9) Balazs, A. C.; Ginzburg, V. V.; Qiu, F.; Peng, G.; Jasnow, D. J. *Phys. Chem. Part B* **2000**, *104*, 3411–3422.
(10) Ginzburg, V. V.; Peng, G.; Qiu, F.; Jasnow, D.; Balazs, A. C. *Phys. Rev. E* **1999**, *60*, 4352–4359.
(11) Wang, Y.; Zhang, Q.; Fu, Q. *Macromol. Rapid Commun.* **2003**, *24*, 231–235.
(12) Fu, Q.; Zhang, Q.; Yang, H. *Polymer* **2004**, *45*, 1913–1922.
(13) Yurekli, K.; Karim, A.; Amis, E. J.; Krishnamoorti, R. *Macromolecules* **2003**, *36*, 7256–7267.
(14) Yurekli, K.; Karim, A.; Amis, E. J.; Krishnamoorti, R. *Macromolcules* **2004**, *37*, 507–515.
(15) Han, C. C.; Okada, M.; Muroga, Y.; McCrackin, F. L.; Bauer, B. J.; Tran-Cong, Q. *Polym. Eng. Sci.* **1986**, *26*, 3–8.
(16) Nishi, T.; Wang, T. T.; Kwei, T. K. *Macromolecules* **1975**, *8*, 227–234.
(17) Yang, H.; Shibayama, M.; Stein, R. S.; Shimizu, N.; Hashimoto, T. *Macromolecules* **1986**, *19*, 1667–1674.
(18) Rinaldi, P. L.; Wagler, T.; Han, C. D.; Chun, H. *Macromolecules* **2000**, *33*, 1778–1789.
(19) Shibayama, M.; Yang, H.; Stein, R. S.; Han, C. C. *Macromolecules* **1985**, *18*, 2179–2187.
(20) Mabrouk, K. E.; Bousmina, M. *Rheol. Acta* **2006**, *45*, 959–969.
(21) Arnauts, J.; De Cooman, R.; Vandeweerdt, P.; Koningsveld, R.; Berghmans, H. *Thermochim. Acta* **1994**, *238*, 1–16.
(22) Kinzer, K. E.; Lloyd, D. R. *Polym. Mater. Sci. Eng.* **1989**, *61*, 794–798.
(23) Mabrouk, K. E.; Bousmina, M. *Rheol. Acta* **2006**, *45*, 877–889.
(24) Chopra, D.; Kontopoulou, M.; Vlassopoulos, D.; Hatzikiriakos, S. G. *Rheol. Acta* **2002**, *41*, 10–24.
(25) Kim, J. K.; Son, H. W. *Polymer* **1999**, *40*, 6789–6801.
(26) Kim, J. K.; Son, H. W.; Lee, Y.; Kim, J. J. *Polym. Sci., Part B: Polym. Phys.* **1999**, *37*, 889–906.
(27) Takahashi, Y.; Suzuki, H.; Nakagawa, Y.; Noda, I. *Macromolecules* **1994**, *27*, 6476–6481.
(28) Jeon, H. S.; Nakatani, A. I.; Han, C. C.; Colby, R. H. *Macromolecules* **2000**, *33*, 9732–9739.
(29) Nesarikar, A. R. *Macromolecules* **1995**, *28*, 7202–7207.
(30) Polios, I. S.; Soliman, M.; Lee, C.; Gido, S. P.; Schmidt-Rohr, K.; Winter, H. H. *Macromolecules* **1997**, *30*, 4470–4480.
(31) Winter, H. H.; Mali, S.; Malone, M. F.; Halary, J. L.; Monnerie, L. *Macromolecules* **1991**, *24*, 5451–5458.
(32) Kapnistos, M.; Vlassopoulos, D.; Anastasiadis, S. H.; Stammer, A.; Wolf, B. A. *Macromolecules* **1996**, *29*, 7155–7163.
(33) Vinckier, I.; Laun, H. M. *Rheol. Acta* **1999**, *38*, 274–286.
(34) Zhang, Z. L.; Zhang, H. D.; Yang, Y. L.; Vinckier, I.; Laun, H. M. *Macromolecules* **2002**, *34*, 1416–1429.
(35) Bousmina, M.; Lavoie, A.; Riedl, B. *Macromolecules* **2002**, *35*, 6274–6283.
(36) Steinmann, S.; Gronski, W.; Friedricsh, C. *Rheol. Acta* **2002**, *41*, 77–86.
(37) Nishi, T.; Wang, T. T.; Kwei, T. K. *Macromolecules* **1975**, *8*, 227–234.
(38) Hashimoto, T.; Itakura, M.; Hasegawa, H. J. *Chem. Phys.* **1986**, *85*, 6118–6128.
(39) Zhi-Gang, Wang.; Yan-Hua, Niu. *Macromolecules* **2006**, *39*, 4175–4183.
(40) Perti, H. M.; Stammer, A.; Wolf, B. A. *Macromol. Chem. Phys.* **1995**, *196*, 1453–1463.
(41) Ganesan, V.; Pryamitsyn, V. *Macromolecules* **2006**, *39*, 844–856.
(42) Tanaka, H. *Phys. Rev. Lett.* **1996**, *76*, 787–790.
(43) Ajji, A.; Choplin, L. *Macromolecules* **1991**, *24*, 5221–5223.
(44) Fredrickson, G. H.; Larson, R. G. *J. Chem. Phys.* **1987**, *86*, 1553–1560.
(45) De Gennes, P. G. *Scaling Concepts in Polymer Physics*; Cornell University Press: Ithaca, NY, 1979.
(46) Brandrup, J., Immergut, E. H., Grulke, E. A., Eds.; *Polymer Handbook*, 4th ed.; Wiley-Interscience: New York, 1999.
(47) Wu, W.; Glese, R. F.; VanOss, C. J. *Langmuir* **1995**, *11*, 379–382.
(48) Brown, D.; Mele, P.; Marceau, S.; Alberola, N. D. *Macromolecules* **2003**, *36*, 1395–1406.
(49) (a) Kim, B. J.; Given-Beck, S.; Bang, J.; Hawker, C. J.; Kramer, E. J. *Macromolecules* **2007**, *40*, 1796–1798. (b) Park, S. C.; Kim, B. J.; Hawker, C. J.; Kramer, E. J.; Bang, J.; Ha, J. S. *Macromolecules* **2007**, *40*, 8119–8124. (c) Costanzo, P. J.; Beyer, F. L. *Macromolecules* **2007**, *40*, 3996–4001. (d) Kim, B. J.; Bang, J.; Hawker, C. J.; Kramer, E. J. *Macromolecules* **2006**, *39*, 4108–4114.
(50) (a) Liu, Y. L.; Hsu, C. Y.; Su, Y. H.; Lai, J. Y. *Biomacromolecules* **2005**, *6*, 368–373. (b) Liu, Y. L.; Su, Y. H.; Lai, J. Y. *Polymer* **2004**, *45*, 6831–6837.
(51) Polios, I. S.; Soliman, M.; Lee, C.; Gido, S. P.; Schmidt-Rohr, K.; Winter, H. H. *Macromolecules* **1997**, *30*, 4470–4480.

MA7020985